IEEE Access
Multidisciplinary | Rapid Review | Open Access Journal

SPECIAL SECTION ON ENERGY HARVESTING TECHNOLOGIES FOR WEARABLE AND IMPLANTABLE DEVICES

Received August 31, 2020, accepted September 9, 2020, date of publication September 15, 2020,
date of current version September 28, 2020.

Digital Object Identifier 10.1109/ACCESS.2020.3024167

Prediction of Harvestable Energy for Self-Powered Wearable Healthcare Devices: Filling a Gap

MARAM A. WAHBA[1], AMIRA S. ASHOUR[1], AND RAMI GHANNAM[2], (Senior Member, IEEE)

[1]Department of Electronics and Electrical Communications Engineering, Faculty of Engineering, Tanta University, Tanta 31527, Egypt
[2]Microelectronics Lab, Electronics and Nanoscale Engineering Research Division, School of Engineering, University of Glasgow, Glasgow G12 8QQ, U.K.

Corresponding author: Maram A. Wahba (maram_ahmed@f-eng.tanta.edu.eg)

This work was supported by UK's Engineering and Physical Sciences Research Council (EPSRC) under Grant EP/R511705/1.

ABSTRACT Self-powered or autonomously driven wearable devices are touted to revolutionize the personalized healthcare industry, promising sustainable medical care for a large population of healthcare seekers. Current wearable devices rely on batteries for providing the necessary energy to the various electronic components. However, to ensure continuous and uninterrupted operation, these wearable devices need to scavenge energy from their surroundings. Different energy sources have been used to power wearable devices. These include predictable energy sources such as solar energy and radio frequency, as well as unpredictable energy from the human body. Nevertheless, these energy sources are either intermittent or deliver low power densities. Therefore, being able to predict or forecast the amount of harvestable energy over time enables the wearable to intelligently manage and plan its own energy resources more effectively. Several prediction approaches have been proposed in the context of energy harvesting wireless sensor network (EH-WSN) nodes. In their architectural design, these nodes are very similar to self-powered wearable devices. However, additional factors need to be considered to ensure a deeper market penetration of truly autonomous wearables for healthcare applications, which include low-cost, low-power, small-size, high-performance and lightweight. In this paper, we review the energy prediction approaches that were originally proposed for EH-WSN nodes and critique their application in wearable healthcare devices. Our comparison is based on their prediction accuracy, memory requirement, and execution time. We conclude that statistical techniques are better designed to meet the needs of short-term predictions, while long-term predictions require the hybridization of several linear and non-linear machine learning techniques. In addition to the recommendations, we discuss the challenges and future perspectives of these technique in our review.

INDEX TERMS Wearable devices, energy harvesting, healthcare, wireless sensors, energy prediction.

I. INTRODUCTION

For better management of chronic diseases such as ischemic heart diseases and diabetes, the demand for developing personalized real-time patient monitoring systems is critical [1]. Recent advancements in microelectronics, mobile computing, as well as the internet of things (IoT), and artificial intelligence (AI) technologies have significantly contributed to the emergence of wearable sensing devices. The wide potential of this unique sensing platform in several applications, including health monitoring, medical prosthetics and consumer electronics, have motivated tremendous research efforts in this domain [2]. Additionally, the wearable medical sensors market is expected to gain momentum, as the market size is anticipated to reach 139,353.6 million USD by 2026, which demonstrates a 467.13 % growth in the market size compared to 2018 [3]. Wearable devices encompass an array of miniaturized sensors, a wireless transmission module, a power supply module, and electronics for data acquisition and processing, which are all packaged in a supportive wearable encasing such as a glove [4], [5], wristband [6], [7], contact lens [8], [9], or a ring [10], [11]. These portable units can gather the patients' physiological signals and periodically transmit them through a wireless network

The associate editor coordinating the review of this manuscript and approving it for publication was Abdul Halim Miah.

to the remote healthcare service provider. The recorded data is then processed for detecting and predicting acute health events, which lead to fast medical intervention in such cases.

Nevertheless, the widespread adoption of self-powered wearable devices for healthcare applications is limited by several factors that include their size, ease of use, cost, and their energy sustainability [12]. Batteries are the most common energy source for wearable devices, but their use impedes perpetual operation due to the battery's limited lifetime [13], which means that frequent recharging or replacement is necessary. In this regard, energy harvesting from the surroundings or from the human body is considered a promising method for deepening the penetration of self-powered wearable devices for patient monitoring using power-efficient and self-sustainable portable devices [14].

Energy harvesting is the process of converting the ambient or external energy into useful electricity. This process will not completely avoid the need for batteries or other energy storage technologies in wearables, but it will effectively reduce their reliance on such technologies as their single source of energy. There are several types of energy harvesting techniques that have been proposed in the literature, which are based on converting light, heat, mechanical, electromagnetic, wind, acoustic, and biochemical energy into electricity. Furthermore, hybrid techniques, which combine different energy sources on a single platform have previously been demonstrated [15]. However, in the context of self-powered wearable devices for healthcare applications, the most common sources are solar irradiation [16], radio frequency (RF) [17], thermoelectric energy [18], and mechanical [19] energy owing to their large power conversion density, which is an important attribute for achieving lightweight and small-sized wearable devices.

Despite their potential and due to the fluctuating nature of these energy sources, all the previously mentioned energy harvesting techniques are either location or time dependent. Consequently, this uncertainty in harvestable energy will always impact the performance of wearable healthcare devices. In this regard, accurately predicting the amount of harvestable energy from the human body, as well as the wearable's surroundings will enable it to effectively manage its current energy reserves for future use. This helps avoid temporary energy shortages falling below a critical level. It also opens the door to additional functionalities that can be implemented on the wearable device, especially if energy demand is variable.

Accordingly, several energy prediction models have been proposed in the literature, particularly for solar energy [20]. The power management technique based on energy prediction can overcome the problem of the harvested power variation over time by taking decisive actions and allowing the system to efficiently exploit the available energy. Other power management techniques were proposed for the efficient use of un-predictable energy sources, such as the thermal, and mechanical energies [21]. Despite the importance of power management models in wearable technologies, very few studies were conducted in this domain. Consequently, based on the architectural resemblance of wireless wearables and wireless sensor nodes, this study investigates the most prominent prediction methods in energy harvesting wireless sensor networks (EH-WSNs). We investigate the relative advantages of each mechanism, while only considering the energy sources that are commonly harvested in wearables. Thus, an overview of the main proposed energy predictors for photovoltaic and RF energy harvesters in EH-WSN literature are presented, since these energy sources are the predictable energy harvesting sources for wearable devices.

The remainder of this paper is organized as follows. Section II provides the system architecture of typical EH-WSN nodes. Our focus in this article is on the Power Management Subsystem shown in Fig. 1. Next, in Section III we provide a comparison between the energy harvesting sources, as well as the technologies used for self-powered wearable healthcare devices. In section IV we critically analyze and compare the different methods for predicting the amount of harvestable energy in self-powered wearable devices. Moreover, we provide recommendations and future directions in section V of the article. Finally, the article ends with concluding remarks in section VI.

II. SYSTEM ARCHITECTURE OF ENERGY HARVESTING WIRELESS SENSOR NODES

The system architecture of energy harvesting wireless sensor nodes comprises four main subsystems, namely data acquisition, processing and storage, radio, and power management subsystems [15] as outlined in Fig. 1.

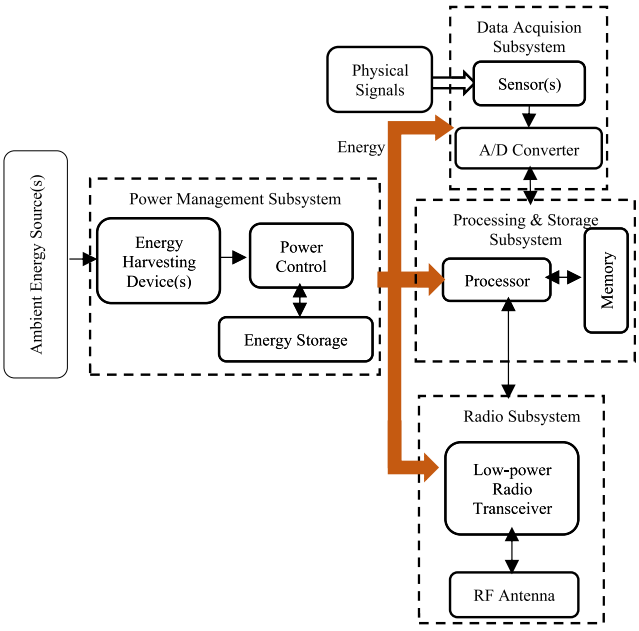

FIGURE 1. Schematic diagram of energy harvesting wireless sensor node.

In the data acquisition subsystem, the sensor detects the physical signal, which is inputted to the analog-to-digital converter to convert the output of the sensor into its digital form. The converted signal is then fed to the processing and storage

subsystem. The main purpose of the processor is to execute the instructions pertaining to sensing, communication and self-organization. Additionally, it interconnects the other subsystems, and any additional peripherals, such as the localization units. The storage process has two-folds: non-volatile memory to store the application-related data, and an active memory which temporarily stores the sensed data and the internal clock. It is a good practice to deploy low-power microcontrollers in the processing and storage subsystem of the wireless sensor nodes due to their small size, low-power consumption, low-cost, and compact construction compared to the field-programmable gate arrays (FPGAs) [22]. The radio subsystem uses low-power transceivers, and radio frequency antennas to connect the node to the WSN gateway in case of point-to-point communication, or to the other WSN nodes creating a mesh.

The most crucial consideration in the design and operation of wireless sensor (WS) nodes is the tradeoff between their energy requirements and their performance. Hence, the power management system in EH-WSN nodes alleviate the dependency on a fixed or finite energy source by incorporating energy harvesters, which scavenge ambient, external, or human-generated energy and transduce them into electrical energy. This energy is then transferred to the power control unit, which regulates the energy storage and consumption process. Decisions are then made to directly power the subsystems using the harvested energy or to buffer the energy at the energy storage unit. The architecture of the power management subsystem is represented in more details in Fig. 2.

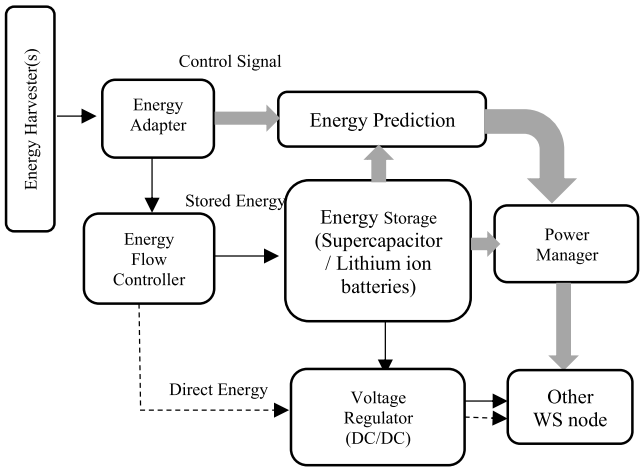

FIGURE 2. Schematic diagram of power management subsystem of energy harvesting wireless sensor node.

From Fig. 2, one or multiple energy harvesters may be used in the power management subsystem to scavenge energy from different sources. For example, photovoltaic cells and thermoelectric generators [23] can be used for harvesting solar and thermal energies. Using this approach, an energy adapter is required for normalizing the output energy from different energy harvesters. Afterward, the energy flow controller distributes the obtained energy to satisfy two scenarios, namely i) when the harvested energy is available, the obtained energy is directly used to power the WSN node through a DC/DC converter that regulates the provided voltage, and ii) if the harvested energy exceeds the consumed energy, this surplus is accumulated in the energy buffer for later use at times of scarce harvesting resources.

Commonly, rechargeable batteries and supercapacitors are used in the energy storage unit. However, many EH-WSNs rely on supercapacitors, either as a standalone energy buffer [24], [25], or in combination with batteries [23], [26]. This is due to their several advantages compared to rechargeable batteries, including higher lifetime, simpler charging circuits, and higher charging/discharging efficiencies. Both types of storage units suffer from self-discharge and leakage, which cause a reduction in their stored energy due to chemical factors and temperature, even though the storage devices are not in use [27]. Comparing the two approaches (i.e. direct use of energy, and stored energy), the direct use of energy is the most energy efficient as it alleviates the energy loss in the storage units. However, in terms of practicality, the stored energy approach is more realistic due to the fluctuating nature of the energy sources over time, which constrains the rate and the amount of the scavenged energy. Accordingly, intelligent power management techniques such as energy prediction are crucial for estimating energy availability and forecasting energy intake. Moreover, the efficient use of available energy sources enables the EH-WSN node to dynamically adjust its wake-up intervals to satisfy energy neutral operation (ENO) [26].

In the following section, we describe the most common energy sources in the context of self-powered medical wearables. We compare their average power densities, conversion efficiencies, and classify them in terms of their controllability and predictability. We will subsequently review the energy prediction approaches in Section IV.

III. COMPARISON BETWEEN ENERGY HARVESTING TECHNIQUES IN SELF-POWERED WEARABLES

Sources for energy harvesting applications can be classified as either ambient-, or human-based energy sources. Despite the wide variety of ambient energy sources, they are either location or time dependent. Some of these sources have a further reduced availability in indoor environments, which is where most wearables are typically used. The most popular energy harvesting technologies rely on converting light, heat, radio frequency and body movements into electricity [28]. We will therefore discuss the most common materials and architectures used in each of these technologies.

Photovoltaic (PV) energy harvesting from solar and indoor light has shown great potential, especially following recent advances in power density, flexibility, and sensitivity [29], [30]. Such technologies rely on converting the Sun's energy into electricity using materials that produce currents and voltages as a result of light absorption. Semiconducting materials are typically used, with power densities reaching 15 mW/cm^2 for outdoor applications [15]. However, despite their high efficiency, photovoltaic energy harvesting

using rigid semiconducting materials is not ideal for wearable applications. Thus, flexible non-crystalline materials are currently being investigated for wearable applications. For example, a flexible perovskite solar cell with an integrated lithium ion capacitor has been demonstrated by Li *et al.* [31]. Their strain sensing device can be integrated into garments and has shown an efficiency of 8.4%. A schematic diagram illustrating the concept is shown in Fig. 3a. Methods for improving the efficiency of such devices as well as their long-term stability are still under investigation, as mentioned in the review by Hashemi *et al.* [32].

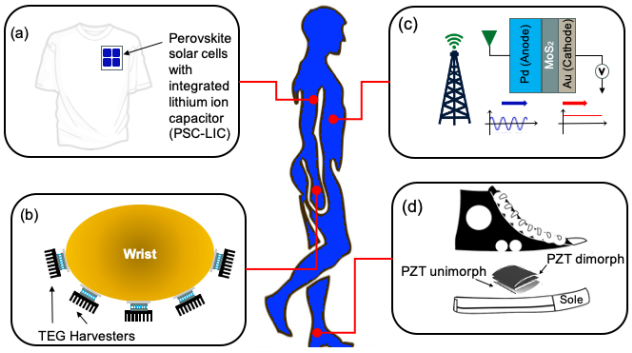

FIGURE 3. Schematic diagram of different energy harvesting methods from the human body and its surroundings. These include (a) Solar energy conversion using flexible materials [31], (b) TEGs on the wrist [28], (c) RF harvesters on flexible substrates [40], and (d) Piezoelectric harvesters embedded in shoes [38].

On the other hand, body heat and body movements are practical energy sources for wearable devices. For example, body thermal radiation can be harvested using thermoelectric generators, which rely on temperature gradients in ceramics, polymers and semiconducting materials for electricity production. Here, the Seebeck effect is responsible for converting this temperature difference into a potential difference. Therefore, heating one end of the thermoelectric material causes carriers to diffuse from the cold to the hot ends of the material [14]. Needless to mention that semiconducting materials such as Bismuth Telluride have been widely used for thermoelectric applications due to their low cost and high Seebeck Coefficient [33]. Moreover, thermoelectric generators (TEGs) for healthcare applications have been demonstrated by Thielen *et al.*, which were subsequently combined with DC-DC converters to provide a power density ranging from 13 to 14 μW/cm^2. Despite this low power density, their lightweight bracelet system consisting of multiple TEGs wrapped around the wrist proves that sensors can be powered using such a device [28]. Figure 3b illustrates the underlying concept of their harvester.

Moreover, researchers exploited the mechanical and kinetic energy from human movements and vibrations to power wearable devices using piezoelectric, electrostatic, electromagnetic, and triboelectric energy harvesting techniques [34]. Materials that have been used for piezoelectric applications include Zinc Oxide (ZnO) and Zirconate Titanate (PZT) [35]. Currently, the most effective method of harvesting kinetic energy from the human body is from walking [36]. According to the literature, almost 67 W of power can be generated from a person weighing 68 kg walking at a speed of two steps per second [37]. For example, a PZT dimorph was inserted under the heel to produce 8.4 mW for a 500 kΩ load and a walking rate of 0.9 Hz [38].

Furthermore, RF energy, at the frequency band from 3 KHz to 30 GHz, was used for powering several wearable devices by developing custom-built rectennas suitable for harvesting ambient wireless transmissions. These ambient transmissions include the radio and television broadcasting, Wi-Fi communications, mobile transmissions microwaves. However, Wi-Fi communications are the most common source for RF energy harvesting due to their wide availability and their closer proximity to the user's wearable device compared to the other ambient sources [39]. An example of such a flexible device has been demonstrated by Zhang *et al.*, where rectennas were used to convert RF energy from Wi-Fi into electricity [40]. Their device consisted of a Molybdenum disulfide (MoS_2) semiconducting–metallic-phase heterojunction with a cutoff frequency of 10 GHz, which is ideal for harvesting electromagnetic radiation from Wi-Fi systems that typically operate in the 2.5 to 6 GHz range. Thus, an incident electromagnetic wave can be converted into direct current. The MoS_2 Schottky diode structure is shown in Fig. 3c, which includes a metal palladium (Pd) anode and a gold (Au) Ohmic contact that serves as the cathode. Their device demonstrated a high power conversion efficiency of 40.1%. Despite the ubiquitous nature of RF radiation, such harvesters still suffer from low output power (62 μW).

Other human movement methods have been investigated by Halim *et al.*, where the swing motion of arms during walking was converted to useful electricity (between 55 to 61 μW) using an electromagnetic energy harvester [41], [42]. The architecture of the electromechanical transducer consisted of two eccentric rotors containing five magnetic pole pairs and an array of coils in the middle.

Recently, there has been an increased interest in developing hybrid energy harvesters, which scavenge energy from multiple sources to mitigate the limitations of each other. An example of this is the smart bracelet device demonstrated by Magno *et al.*, which combines both thermoelectric and photovoltaic energy harvesters [43]. The heart of this complete wrist-worn system is an ultra-low power processor (Mr. Wolf), which receives power from a dual harvester consisting of flexible solar cells and a TEG harvester.

Table 1 compares the different energy harvesting techniques for self-powered medical wearables in terms of their advantages and limitations, indicating the typical power densities produced using these techniques. Given the dynamic nature of these energy sources, the rate and the amount of harvestable energy varies with time, which increases the need for efficient power management in terms of energy use and storage. This is to ensure sustainable operation of the energy harvesting devices.

TABLE 1. Comparison between energy harvesting methods for self-powered wearable healthcare devices.

Energy Source	EH technique	Typical harvested power density	Advantages	Limitations for application
Light energy Human body thermal energy	Photovoltaic	Outdoors (direct sun): 15 mW/cm^2 [15] Outdoors (cloudy day): 0.5 mW/cm^2 [44] Indoors (using light): up to 30 $\mu W/cm^2$ [44] Indoors (using human infrared thermal emissions): 2.2 $\mu W/cm^2$ [14]	Scalability Low cost Maintenance free No moving parts Simple design High power density Easy fabrication High availability Reliability	Fabrication material selection Surface area Amount of illumination Device location
Human body thermal energy	Thermoelectric	Human (indoors): 60 $\mu W/cm^2$ [14] Human (at 0 °C ambient): 97.2 mW/cm^3 [45]	Scalability Low cost Maintenance free No moving parts Simple design High availability and reliability Output power independent on size	Low efficiency Requires a mechanism to maintain the temperature difference across the device Works best outdoors
Human body mechanical energy	Piezoelectric	~68 $\mu W/cm^2$ [46]	Simple technique Small size High output voltage Power density	Low efficiency at low-frequency Requires frequency up-conversion Fabrication material selection Low output current
	Electrostatic	~ 0.1 $\mu W/cm^2$ for implantables and 1.2 $\mu W/cm^2$ for wearables [14]	Compatible with MEMS technology Easy fabrication Good performance at low-frequency vibrations	Need start-up voltage Complexity Capacitance range of variation affects efficiency and energy gain Electret discharge for liquid-based harvesters
	Electromagnetic	~ 4 $\mu W/cm^3$ from human motion [14]	Durable operation High output current No mechanical parts No external voltage source	Bulkiness Challenging to miniaturize Affected by vibration amplitude, frequency, and damping factor Difficult to make microscale coil, low flexibility Low output voltage
	Triboelectric	~ 36 mW/cm^2 [47]	Very high output voltage, and power density, simple, ease of fabrication, scalability, cost-effective, flexibility	Electrostatic charge Low current density, performance dependent on the choice of materials Temperature Surface roughness, and strain Requires surface morphology modification
Radio Frequency Energy	Rectennas	~ 0.01- 0.1 $\mu W/cm^2$ for distances ranging from 25 m to 100 m from a GSM base station [14]	Widely available over a large frequency range Simple circuits as series RF-DC converters provide good compromise between conversion efficiency and output voltage	Low power density Varies with distance Short range Transient drops in received power level may occur because of different radio wave propagation phenomena and traffic fluctuations

IV. REVIEW OF ENERGY PREDICTION METHODS

Energy prediction methods can be used to forecast energy source availability and evaluate the expected energy intake. This allows the energy harvesting system to efficiently manage its own resources and store enough energy for any unexpected energy dips. The energy sources used in self-powered medical wearables are classified according to their predictability and controllability [21], as reported in Table 2. Controllable energy sources do not require energy forecasting, due to their on-demand availability. On the other hand, the ability to predict the availability of non-controllable energy source using energy prediction techniques supports the efficient power management of EH-based devices.

TABLE 2. Predictability vs controllability of energy harvesters for wearable healthcare devices.

Energy source	Predictability	Controllability	Conversion efficiency	Examples of proposed devices
Photovoltaic	√	×	25±1.5% [48]	InfiniWolf smart bracelet [49], flexible pulse-oximeter bracelet [50], solar-powered converter for wearable devices [51], wearable electromyography wristband [52]
Radio Frequency	√	√	50% excluding transmission efficiency [15]	WiWear [39], dual-band wearable rectenna [53], wearable rectenna for healthcare [40, 54]
Human-based physiological	×	×	5-30% [55]	Human temperature-based wearables [18, 28, 56], wearable thermoelectric-based electrocardiography [57]
Human-based activity	×	√		Human motion wearable piezoelectric harvesters [58-61]

Energy prediction methods are based on using available historical time-series datasets and meteorological parameters to efficiently forecast the available energy at upcoming time intervals. The existing prediction models can be divided into three main classes, as shown in Fig. 4: statistical, stochastic, and machine learning models. The performance of these prediction classes and their specific methods vary in terms of prediction accuracy, the required memory, and the execution time, which are critical in evaluating the adequacy of such methods in energy prediction for wearable devices.

However, few studies in the literature have considered energy prediction for wearable devices. Therefore, based on the architectural resemblance of wearable devices to EH-WS nodes, the energy prediction methods proposed for the latter have been investigated in this study to determine their effectiveness for wearable devices. From this deduction, the energy prediction methods for EH sources that are commonly used by wearable devices would be only considered. For example, energy prediction for wearable devices is critical in the following cases:

- In case of predicting the time-ahead scarcity of solar energy, the device regulates the currently available energy to maximize the preserved energy at the secondary storage for further use at the time of need. Also, task scheduling, and adaptive duty cycle management at the media access control (MAC) layer of the device would be set accordingly [62].
- In case of predicting the RF link quality, the device can estimate the remaining RF connectivity time for

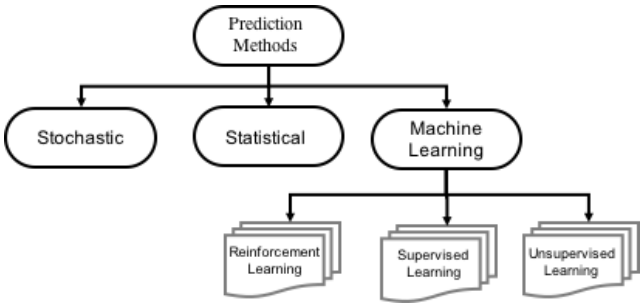

FIGURE 4. Different classes of prediction models.

avoiding the unnecessary message transmissions. Thus, fully exploiting the available energy in transmitting the critical data, minimizing the wasted energy, and optimizing the network performance [63].

Thus, an overview of energy predictors for photovoltaic and RF energy harvesters in EH-WSN literature are presented, since these energy sources can be predicted in autonomous or self-powered wearable devices.

A. STATISTICAL METHODS

Statistical models adopt different statistics such as mean, variance, standard deviation, and moving average to estimate the available energy at a particular time interval based on the given historical energy profiles. The exponentially weighted moving-average (EWMA) model, which is considered as the baseline of statistical-based prediction models, was applied in predicting the availability of solar energy. This model relies on the rough assumption, where the generated energy profiles of the consequent days have similar distribution over the corresponding time intervals. This means that the available energy at a specific time interval during the day is related to the observed energy during the same time interval in the previous days. Thus, based on the stored historical summary of the energy generation profiles, the expected energy at a certain slot during the current day is an exponentially weighted moving average of the energy during the same slot for the previously observed days. Subsequently, each day is discretized into N equal-length time slots, usually about 30 minutes each, yielding to 48 slots [64]. However, the selection of the slot length considers the tradeoff between the uniformity of the solar activity during each slot, which is achieved by selecting shorter slots, and the memory overhead caused by the storage of a large number of slots (N-sized vector), as shorter slots lead to higher N. The EWMA model predicts the amount of energy $\widehat{E}$ in the nth time slot, as follows [65]:

$$\widehat{E}_n^d = \alpha.\widehat{E}_n^{d-1} + (1-\alpha).M_n \tag{1}$$

where d represents the current day, M_n represents the average value of the harvested energy at the nth slot for the previous days, and α is the weighting factor ($0 < \alpha < 1$) to ensure less contribution of the older days to the progression of the predicted value. The study of Kansal *et al.* [64] compared the effect of different values of α on the prediction error have suggested an optimal value of $\alpha = 0.5$, whereas another study was proposed using smaller values of α (i.e. $\alpha = 0.3$) for the fast adaptation to seasonal changing [66]. Similar to the EWMA, the Swiss Federal Institute of Technology Zurich (ETHZ) prediction method [67], which can be used for both short term and long term predictions, included the data collected over the past days in an exponentially decaying manner, along with the received energy in the current time slot. However, the ETHZ method is comparably more complex in terms of the number of multiplications, and the required prediction time. The derived short term predicted energy is a weighted combination of the following three values, namely the measured energy at the previous slot, the average incoming power at the last T samples, and the short-term energy average. The last two values are also multiplied by weighting coefficients. The main drawback of the EWMA is the inability to adjust well to the frequent variations of weather conditions, such as the alternation of cloudy and sunny days, causing an average error of 30% between the predicted and the true harvested energy [68]. This was the main motivation behind developing the weather-conditioned moving average (WCMA) model which accounts for weather turbulence by including the weather conditions of the current day, as described by the following expression [68]:

$$\widehat{E}_n = \alpha.E_{n-1} + (1-\alpha).M_n GAP^K \tag{2}$$

where E_{n-1} is the last harvested energy, and M_n is the mean of the stored energy values E at the time slot (n) for the D previous days, which is given as follows:

$$M_n = \frac{\sum_{i=d-1}^{d-D} E_n^{(i)}}{D} \tag{3}$$

For the n^{th} slot, the GAP factor estimates the current day weather conditions based on the ratio between the measured energy of the K previous time slots [*n-K+1, . . . , n-1*] on the current day to their average estimated energy values over the previous D days. For computing this factor, two K-element vectors were defined, namely $V = [v_1, v_2, \ldots, v_K]$ and $P = [p_1, p_2, \ldots, p_K]$, which indicate the energy quotient of the prior samples and their weights, respectively, as follows [68]:

$$v_k = \frac{E_{n-K+k-1}}{M_{n-K+k-1}} \tag{4}$$

$$p_k = \frac{k}{K} \tag{5}$$

The P vector has the weights assigned to the K previous slots, which are in proportion to their proximity to the n^{th} time slot, such that the most recent slots have larger weights and higher contribution to its expected weather condition. Subsequently, the GAP is computed as follows:

$$GAP^K = \frac{V.P}{\sum_{k=1}^{K} p_k} \tag{6}$$

Thus, the higher memory requirement of WCMA compared to the EWMA is due to its storage of the measured energy matrix $E(i,j)$, where j is the number of the time slot at the

i^{th} day. Moreover, the significant changes in the solar condition at sunrise and sunset using the WCMA lead to peaking the prediction error at these times, especially for weighting factor values of $\alpha > 0.5$, as the preceding slots contribute to the current slot prediction [67]. The prior setting of this factor generally tunes it for a particular set of data to justify the current measurements along with the historical data, which does not necessarily ensure the fast adaptation to the rapidly changing weather conditions. Therefore, several algorithms were proposed for addressing this issue, such as the dynamic WCMA (D-WCMA) at which α is adapted dynamically according to the mean value of the historical data [69]. For further improvement in the prediction accuracy, the last observation E_{n-1} was replaced by a linear weighted combination of the last observation and the closest energy pattern in the stored data, which was proposed by the universal dynamic WCMA (UD-WCMA). Also, Bergonzini *et al.* [67] proposed the WCMA-PDR algorithm including phase displacement regulator for reducing the prediction error over the consecutive days through exploiting the prediction errors of the past days in a feedback manner, which reduced the prediction error to 9.2% compared to 10% for the WCMA, while increasing the memory requirement by 25% and the time for prediction by 62.7%.

The statistical profile-energy (Pro-Energy) energy prediction model [70] was proposed for predicting the short-term (30 minutes) and the medium-term (one hour to couple of hours) energy generation. Similar to the WCMA, the Pro-Energy maintains the recorded energy generation profiles of the previously observed D days, which are used for estimating the future energy intake. Similar to the prementioned models, each day is divided into N equal-sized time slots, which are usually 30 minutes each (i.e. 48 time slots). The predicted values during the N slots of the current day are stored in an N-dimensional vector. The energy profiles of the previously observed days are stored in a $(D \times N)$ matrix. Unlike the prementioned models that depend on the energy intake of the previous days, the Pro-Energy model search in the pool of the previously stored energy profiles to find the profile with the highest similarity to the current day and exploiting it in the energy prediction of the next time slot. Accordingly, the forecasted energy for the time slot $(n + i)$ at the current day d is described over the short-term and medium term, respectively, as follows:

$$\widehat{E}^{d}_{n+1} = \alpha.E^{d}_{n} + (1-\alpha).E^{d^*}_{n+1} \tag{7}$$

$$\widehat{E}^{d}_{n+i} = \gamma_i.E^{d}_{n} + (1-\gamma_i).E^{d^*}_{n+i} \tag{8}$$

where i is the i^{th} timeslot with respect to n, E^{d}_{n} is the energy harvested at the n^{th} slot during the current day (d), α and γ are weighting factors, and $E^{d^*}_{n+i}$ is the energy harvested at the $(n + i)$ slot at the most similar day (d^*). For indicating the most similar day, the mean absolute error (MAE) is calculated as the difference between the energy predictions of the last observed K timeslots of the current day and the corresponding predictions for each of the recorded D days. Accordingly, the day with the least MAE is determined as the most similar day. Conversely, the variation in the energy harvesting rate throughout the different periods of the day does not guarantee the best prediction results using fixed-length timeslots.

Thus, one of the proposed advancements of the Pro-Energy model is the Pro-Energy model with variable length timeslots (Pro-Energy-VLT) [70], which adapts the granularity of the timeslots (i.e. coarser or finer) according to the dynamics of the energy source. It was reported in the same study that the mean absolute deviation percent (MADP) decreases using a higher number of timeslots, when the harvesting variability is high. For estimating the length of each of the N slots, an iterative algorithm based on the perceptually important point method is applied. This method uses the average daily harvesting profile computed from the historical weather data for estimating the granularity of the timeslots. Also, this model was compared against Pro-Energy, EWMA, adjusted EWMA (AEWMA), and WCMA in terms of the MADP prediction error and memory overhead. In the AEWMA, a scaling factor that represents the ratio between the actual harvested energy and the predicted value for a certain timeslot is used to adjust the future predictions, which accounts for short-term weather variations. Results as shown in Table 3 indicate that Pro-Energy-VLT had less MADP compared to Pro-Energy by 10.1% to 12.3%, 15.9% to 23.1% less than that of WCMA, 35% to 53.2% less than that of AEWMA, and 58.8% to 62.9% less than that of EWMA. The main advantage of this model is reducing the memory requirement and alleviating the overhead of the energy prediction process, which is proportional to the number of timeslots, as Pro-Energy-VLT outperformed Pro-Energy and WCMA in terms of the predictive accuracy, while using nearly half the number of timeslots, which can reduce the memory footprint to more than 40%, as WCMA and Pro-Energy typically consume 20-50% of the total memory available on *Telos B* and *Mica2/MicaZ* motes, respectively.

Another enhancement of the Pro-Energy model is the IPro-Energy model [20], which was proposed for increasing the prediction accuracy and reducing the computational overhead for predictions over both short term and medium term horizons. Instead of selecting the one most similar day from the pool, IPro-Energy minimizes the prediction error by combining the profiles of the two most similar days from the pool in the prediction process (i.e. number of selected profile $P = 2$). These selected profiles are weighted by a factor (w_p) according to their MAE, such that higher weight is assigned to the day profile with the lower MAE, after that the weighted profile (WP) is obtained as follows.

$$w_p = 1 - \left(\frac{MAE_k(O^{d_p}, C)}{\sum_{i=1}^{P} MAE_k(O^{d_i}, C)}\right) \tag{9}$$

$$WP_{n+1} = \frac{1}{P-1} \cdot \sum_{p=1}^{P} (w_p.O^{d_p}_{n+1}) \tag{10}$$

where O^{d_p} is the day p entry at the stored matrix O, $O^{d_p}_{n+1}$ represents the $(n+1)$ timeslot at that entry, and C represents

TABLE 3. Performance summary of the main proposed prediction approaches for EH-WSNs.

Reference	Prediction model	Energy source	Dataset source	Prediction error	Execution time (s)	Memory (Bytes)
[70]	**Pro-Energy-VLT**	Outdoor solar traces (OST) Indoor radiant light (IRL)	OST: traces from Rome (ROME), traces from Oak Ridge, Tennessee(ORNL) [95] IRL: from Energy Harvesting Active Networked Tags project [96]	**OST: 5% ^{ROME} to 11% ^{ORNL} (short-term)** **6% to 14% (medium-term)** **IRL: ~ 24% (short-term)** **~ 31% (medium-term)**	-	1344 (N=32)
	Pro-Energy			OST: 6% to 12% (short-term) 8% to 15% (medium-term) IRL: ~ 28% (short-term) ~ 32% (medium-term)	-	2592 (N=48)
	WCMA			OST: 7% to 18% (short-term) 9% to 25% (medium-term) IRL: ~ 35% (short-term) ~ 45% (medium-term)	-	1732 (N=48)
	AEWMA			OST: 11% to 13% (short-term) 13% to 16% (medium-term) IRL: ~ 30% (short-term) ~ 35% (medium-term)	-	**96 (N=48)**
	EWMA			OST: 11% to 30% (short-term) 10% to 28% (medium-term) IRL: ~ 53% (short-term) ~ 45% (medium-term)	-	**96 (N=48)**
[20]	**IPro-Energy**	Solar irradiance	Traces from New-Mexico (NM), Michigan (MI) [97]	**7.5%^{NM} to 11.9%^{MI} (short-term)** **14.5% to 21.1% (medium-term)** 38.7% to 54.9% (long-term)	0.021	-
	Pro-Energy			15.9% to 24.1% (short-term) 31.1% to 40.9% (medium-term) **35.3% to 53.2% (long-term)**	0.090	-
	WCMA			22.2% to 28.1% (short-term) 84.3% to 96.7% (long-term)	0.014	-
	ASIM			25.9% to 69.8% (short-term) 44.9% to 65.4% (long-term)	**0.013**	-
[90]	Autoregression	Solar irradiance	hourly global solar irradiance ground measurements from Spanish National Radiometric Network stations (AEMet)	20.65% to 25.71% (Murcia) 26.54% to 31.06% (Albacete) 23.11% to 30.10% (Madrid) 23.45% to 29.69% (Lerida)	-	-
	NN			**20.58% to 24.68% (Murcia)** **26.37% to 30.39% (Albacete)** **23.21% to 28.31% (Madrid)** **23.65% to 29.31% (Lerida)**		
	ANFIS			20.86% to 25.69% (Murcia) 27.36% to 30.42% (Albacete) 23.40% to 28.96% (Madrid) 23.52% to 29.66% (Lerida)		

TABLE 3. *(Continued.)* **Performance summary of the main proposed prediction approaches for EH-WSNs.**

[86]	**ALHM**	Solar irradiance	Two-year dataset from the UMASS Trace Repository [98]	**13.68% (long-term) 8.66% to 11.74% (short-term)**	-	-
	NN			18.41% (long-term) 15.24% to 18.84% (short-term)		
	SVM			20.39% (long-term) 16.87% to 21.05% (short-term)		
[84]	**Feedforward NN**	Solar irradiance	Four months dataset from National Renewable Energy Laboratory (NREL)	56.61 W/m^2 (hourly)	-	**20 KB**
	Backpropagation NN			71.47 W/m^2 (hourly)		212 KB
	NARX NN			59.63 W/m^2 (hourly)		216 KB
	Elman backpropagation			66.95 W/m^2 (hourly)		212 KB
	Recurrent NN			**49.17 W/m^2** (hourly)		228 KB
	Model averaged NN			57.82 W/m^2 (hourly)		56 KB
[84]	**Proposed Feedforward NN [84]**	Solar irradiance	Four months dataset from National Renewable Energy Laboratory (NREL)	**56.61 W/m^2** (hourly)	-	**20 KB**
	Adaptive NN + statistical techniques [93]			149.29 W/m^2 (hourly)		228 KB
	Feedforward NN [99]			172 W/m^2 (hourly)		20 KB
	Model averaged NN [83]			204.52 W/m^2 (hourly)		56 KB
[83]	Feedforward NN	Solar irradiance	One year data from Solar Radiation Resource Setup at the Electrical Engineering Department in Madan Mohan Malaviya University of Technology, India	20.5% to 177.88% (over 1-year data)	-	-
	Backpropagation NN			121.74% to 463.12% (over 1-year data)		
	Deep learning NN			140.06% to 241.46% (over 1-year data)		
	Model averaged NN			**35.93% to 120.57% (over 1-year data)**		
[89]	**Hybrid using PME rule**	Solar irradiance	Horizontal global radiation available on the French Meteorological Organization database	**36.59% (hourly NRMSE) 28.39% (daily cumulative NRMSE)**	-	-
	MLP-NN			40.55% (hourly NRMSE) 31.63% (daily cumulative NRMSE)		
	ARMA			40.32% (hourly NRMSE) 32.49% (daily cumulative NRMSE)		
	Persistence			50.62% (hourly NRMSE) 39.94% (daily cumulative NRMSE)		
[88]	**SVM**	Solar irradiance	Research Unit for Renewable Energy Applications (RUREA)	**13.16% (daily prediction NRMSE)**	-	-
	MLP-NN			14.44% (daily prediction NRMSE)		
[100]	**UC-M3**	Solar irradiance	One year hourly GHI and sky imaging dataset by the NREL	**7.94% (hourly NRMSE)**	518 (training) 4.09 (forecasting)	-
	UC-SAML			9.74% (hourly NRMSE)	**220 (training) 3.42 (forecasting)**	

TABLE 3. ***(Continued.)*** **Performance summary of the main proposed prediction approaches for EH-WSNs.**

[101]	**LLR**	Solar irradiance	Traces from the site of the Natural Environment Research Council (NERC) funded hydrological radar experiment (HYREX) project	**19.1 MJ/m^2/day (training)** **22.4 MJ/m^2/day (validation)**	-	-
	MLP (conjugate learning)			28.5 MJ/m^2/day (training) 28.1 MJ/m^2/day (validation)		
	MLP (BFGS)			30.2 MJ/m^2/day (training) 29.7 MJ/m^2/day (validation)		
	ELMAN			32.75 MJ/m^2/day (training) 52.89 MJ/m^2/day (validation)		
	NNARX			26.74 MJ/m^2/day (training) 49.63 MJ/m^2/day (validation)		
	ANFIS			32.14 MJ/m^2/day (training) 65.47 MJ/m^2/day (validation)		
[82]	ARIMA	Solar irradiance	National Environment Agency (NEA)	30% (hourly MAPE)	-	-
	Fuzzy			13.87% - 20.22% (hourly MAPE)		
	NN			10.85% - 20.33% (hourly MAPE)		
	Fuzzy-NN			**6.03% - 9.65% (hourly MAPE)**		
[63]	**GMLA(6) – MM**	RF link quality	Realistic simulations	**1.5%**	-	32 KB
	GMLA(8) – MM			2%		
	GMLA(10) – MM			3.3%		
	GPS – MM			3%		
	BD – MM			13%		
	MTCP - MM			3.3%		
	GMLA(6) – GMM			20%		
	GMLA(8) – GMM			21%		
	GMLA(10) – GMM			23%		
	GPS – GMM			55%		
	BD – GMM			40%		
	MTCP - GMM			50%		
[102]	**O-BD(6)-MM**	RF link quality	Realistic simulations	**2%**	-	-
	O-BD(8)-MM			2%		
	O-BD(10)-MM			4%		
	BD-MM			13%		
	O-BD(6)-GMM			16%		
	O-BD(8)-GMM			17%		
	O-BD(10)-GMM			20%		
	BD-GMM			32%		

the N-dimensional vector that stores the harvested energy values of the current day. The IPro-Energy model uses the smarting factor (S) to incorporate the current day energy pattern based on the harvested energy values of the last two timeslots. Subsequently, the energy prediction for the (n+1) timeslot is obtained for both short-term and medium-term as follows.

$$\widehat{E}^d_{n+i} = W_f.E^d_n + ((1 - W_f).WP_{n+i}) + S \qquad (11)$$

where W_f is a weighting factor ranging between 0 and 1 that enforces the contribution of the current day energy pattern to the predicted value. Table 3 compares the IPro-Energy, Pro-Energy, and WCMA models in terms of their prediction error (according to the mean absolute percentage error (MAPE)), and execution time against the stochastic ASIM model, which is described in the next section.

B. STOCHASTIC METHODS

Stochastic models are based on the stochastic processes to describe the possible fluctuations over time of a random phenomenon, such as the ambient energy availability. Several

studies proposed using first-order Markov chains, a commonly used stochastic process, for predicting solar radiation availability. For instance, Muselli *et al.* [71] proposed coupling Ward's classification method and first-order Markov chains to reproduce the stochastic and statistical properties of the experimental global solar irradiation data, and generate synthesized solar irradiation sequences for sizing PV systems. A two-state first-order Markov model was presented in [72] to model the energy harvesting process of a node, which can be applied to solar EH-WSNs or motion energy harvesting body sensor networks (BSNs). That study modelled the energy harvesting status of a node, as either active or inactive, in addition to the residual energy left in the battery, while considering the presence of sensing events. The performance of the proposed model was verified using the loss probability due to energy run-out (LPERO) and average time to run-out (ATERO) metrics. Besides, Ventura *et al.* [73] proposed MAKERS, a multiple board Markov model for BSN energy harvesting sensors, which integrates both the energy and the traffic models of the node as an extension to the models presented in [72], [74]. It considered that sensors may be equipped with multiple energy harvesting boards allowing them to harvest energy from either a single source, or multiple sources, such as the RF and vibration energy. The performance of the MAKERS model was evaluated using the probability of event-loss due to running out of energy. It was noted that MAKERS model provides less complexity compared to the former models, which facilitates the on-board computations in the sensors. Ku *et al.* [75] modelled the evolution of the solar irradiance during a 10-hour period via a hidden Markov chain whose state parameters, which are the mean μ_j and variance ρ_j of each state, were represented by an underlying normal distribution. The proposed model was trained by an EM model for finding the maximum likelihood estimate of the state parameters based on the observed data. Comparing the histogram of the training result and the observed data, it was observed that the highest similarity between them was obtained after increasing number of states from two to four states, which also increased the system's complexity.

Moreover, Ghuman *et al.* [76] proposed the accurate solar irradiance prediction model (ASIM) based on higher-order Markov chain for high prediction accuracy at the expense of the system complexity. The increase in accuracy is a result of the more accurate state dependencies, considering that the probability of a random process (i.e. solar irradiance level) attaining a state (i.e. a defined range of radiation values) at a particular time instant depends on the attained states at the previous K instants. The prediction accuracy was estimated using the normalized root mean square error (NRMSE) and the percentage of the predicted points within one standard deviation from the corresponding original points of the dataset. The latter metric has increased from 50% with first-order Markov chain to up to 81% using the 10th order model, which also achieved an average NRMSE of 0.78 for the four used datasets. Instead, the implementation complexity presented by the following equation is measured by the number of states (N_S):

$$N_S = \left(\frac{D_{max}}{W}\right)^K \tag{12}$$

where K is the Markov chain order, D_{max} is the maximum irradiance value, and W represent the bin size, which refers to the range of irradiance values considered as a single state. The linear increase in the chain order would result in an exponential increase in the number of states. Nevertheless, it was reported that using third-order Markov chain resulted in an adequately similar performance to the tenth-order model, while requiring 1.43×10^7 times less states, which presents a more viable solution.

As shown in Table 3, the ASIM model was compared to multiple statistical model, namely the IPro-Energy, Pro-Energy, and WCMA in terms of the prediction accuracy, execution time, and their effectiveness when integrated to energy management schemes in [20]. The evaluation of prediction accuracy was performed over the short-term, medium-term, and long-term time horizons due to the significant impact of time horizons on the prediction error. However, ASIM and WCMA were excluded from the medium term comparison due to their design and implementation limitations, while for long-term predictions aggregated energy values of one accumulated value per day were used. It was reported that medium term predictions scored higher mean absolute percentage error (MAPE) values compared to short term predictions, which is due to the higher probability of error accumulation with longer inter-prediction times. With more elaboration, over the short term horizon, IPro-Energy model exhibited the least prediction error compared to the other models, as it had 51%, 60%, and 78% less MAPE compared to Pro-Energy, WCMA, and ASIM, respectively. IPro-Energy exhibited 50% less prediction error compared to Pro-Energy model for solar predictions over the medium-term horizon. Results for long term horizons established the comparable performance of both IPro-Energy and Pro-Energy models which was superior than ASIM and WCMA by 18% and 50%, respectively.

The results established that the highest throughput and active period was achieved without depleting the battery level using IPro-Energy model, followed by the Pro-Energy, WCMA and ASIM models, respectively. Conversely, the ASIM model reported the least execution time, followed by WCMA and IPro-Energy, while Pro-Energy scored the highest execution time. Additionally, IPro-Energy model was more memory efficient compared to the other three models, as IPro-Energy combines only the two most similar days in its prediction calculation. Therefore, it can be concluded that the ASIM model is superior in its fast execution compared to statistical models, while the latter models are more efficient in terms of prediction accuracy and memory requirements, specifically the IPro-Energy model. As the main objective of

energy prediction is to manage the data transmission process of the EH-WSN nodes by regulating the transmission rate and active mode period according to the expected energy availability during a timeslot. Therefore, maximizing the throughput without depleting the energy source, which may occur in case of wrong predictions. Several studies have proposed using Markovian models for tracing the solar irradiance energy pattern of a given dataset in order to model and study several aspects of the EH-WSN nodes, such as the operation of the sensor nodes [77], the evolution of the residual energy and the temporal death probability [78], and finding the optimal transmission policies for maximizing the data throughput [75].

C. MACHINE LEARNING-BASED METHODS

Machine learning (ML) approaches have been effectively tackling key issues in WSNs, which have many applications in the fields of internet of things (IoT), machine communication, and cyber security. These challenging issues include transmission overhead, node localization, node failure, network efficiency, scalability, and reliability. ML is applied to improve the network lifetime by forecasting the available amount of energy at a particular time slot [79]. ML approaches can be categorized into three main categories, supervised learning, unsupervised learning, and reinforcement learning approaches. Supervised approaches are widely adopted in EH- WSNs energy harvesting, while unsupervised models are usually applied in WSN clustering problems. The reinforcement methods are commonly used in prediction-free energy management tasks, such as maximizing the quality of service, while avoiding node death or power failure [80], [81]. In supervised ML approaches, a labeled input-output dataset is applied during the training phase of the system model, which aids in learning the relationship between these input and output data samples. The parameters of the system model are tuned accordingly, allowing the system to estimate the output for the applied blind input samples during the testing phase. ML approaches include supervised neural networks (NN) [82]–[84] deep-learning methods [55], [83], [85], support vector machines (SVM) [85]–[88], and regression methods [85], [89], [90].

1) NEURAL NETWORK-BASED MODELS

In numerical weather prediction (NWP), the time-space domain is discretized on the regional level, and equations of thermodynamics, motion, and mass transfer are then solved for solar intensity forecasting. The physical NWP model and satellite-based approaches were widely adopted for solar forecasting on large temporal and spatial resolutions [91]. On the other hand, numerical weather prediction is based on using composite regional datasets rather than site specific datasets causing error propagation over time steps and node locations. Such a case leads to a root mean square error (RMSE) of 30-50% for day-ahead predictions [92]. Thus, site-specific and intra-hourly forecasts can hardly be precise using NWP or satellite data due to the low image precision and resolution, in addition to infrequent sampling intervals. While, sky imagery-based methods are the most common for intra-hourly forecasts, their prediction accuracy was constrained by several assumptions related to cloud shape and linear cloud movement [93]. Instead, the operation of the neural network was based on local micrometeorological data, which enhanced the local prediction accuracy. Also, its inherent memory enabled recalling the historical anatomies of weather.

These NNs are able to automatically adapt to the long-term and abrupt changes in climatic and environmental conditions. Accordingly, Srivastava *et al.* [83] compared the performance of three NN-based models, namely the feed forward, back propagation, and deep learning NN-based models. These models were compared against the averaged NN model for the 6-day ahead forecasting of the daily solar intensity. Nine parameters were applied as inputs to these models including average, minimum, and maximum temperatures, as well as time, wind, rain, dew point, azimuth angle, and atmospheric pressure. Prediction accuracy was qualified over a one-year dataset and the results in terms of the RMSE are reported in Table 3. Experimental results established that feed forward and model averaging NN models achieved better prediction results compared to the back propagation and deep learning networks in the solar radiation forecasting using the given dataset.

The most influential parameters for global solar radiation (GSR) prediction were studied in [94] for finding the combination of weather parameters that provided the best day-ahead GSR prediction using a three-layer feed forward NN model The day, air temperature, pressure, relative humidity, cloud cover, wind speed, and direction were investigated as input data, which was acquired from real three-year outdoor solar radiation data. The performance evaluation based on the RMSE, MAPE, and correlation coefficient have established that humidity, temperature, and cloud-cover are the optimal features in the GSR prediction, while considering reducing the system's complexity in terms of the number of neurons in the hidden layer. Nevertheless, the cloud-cover data was excluded as it is often unavailable. Hence, the temperature, humidity and day were finally considered as the input data. The proposed model achieved 4.75% RMSE, 3.65% MAPE, and 0.98 correlation factor using 75 neurons in the hidden layer.

Dhillon *et al.* [84] also proposed a feedforward network for the hourly solar irradiance forecasting using three weather parameters, namely pressure, temperature, and relative humidity, which were used for generating a reference signal. The generated reference signal indicated the occurrence probability of cloud formation. Filtration and cross correlation were performed on all the dataset to remove outliers, and determine the optimum filter length for each variable, respectively. Then, features were extracted using independent component analysis (ICA), and then applied to the NN

model, which was trained using the Levenberg-Marquardt (LM) algorithm. Comparisons between different NN models have shown that the most optimal architecture was a two-layer model with 24 neurons at both input and output layers. Although this model provided a 56.61 W/m2 RMSE consuming 20 KBs of memory, only a slight improvement of 4.46 W/m2 in RMSE was obtained using a three-layer model consuming 28 KBs of memory.

Table 3 reports the performance of this proposed model using different types of neural networks and compares the proposed model with other models from literature, where the prediction error is represented by the RMSE in W/m2. It is worth noting that the optimal model choice is based on the tradeoff between the prediction error and model complexity in terms of the occupied memory size. The slight increase in prediction performance is considered insignificant if it comes at the expense of a higher memory demand. The results established the superiority of feedforward networks compared to backpropagation and model averaged NN, which is the same result obtained from [83]. Also for predicting the daily average GSR, Dey *et al.* [85] proposed a 6-layer deep learning-based NN, called SolarisNet. The proposed model was fed using three weather parameters: minimum, maximum, and dry bulb temperatures. The sensitivity analysis of the data showed that the sunshine hour and the minimum temperature features are more significant in the forecasting process compared to the maximum temperature. Also, the experimental results indicated the superiority of the SolarisNet in terms of the prediction accuracy compared to Angstrom-Prescott parametric method, Gaussian process regression, support vector regression, and NN, which was aided by the presence of a non-linear mapping layer in the proposed network for exploiting the non-linear interrelationships among the given parameters. Manjili *et al.* [93] implemented an adaptive framework for day-ahead solar radiation forecasting based on adopting statistical techniques for the selection of the appropriate training sets for the NN model. These statistical techniques included correlation analysis and independent component analysis (ICA) feature extraction from the given 8 weather-related parameters, i.e. temperature, time, relative humidity, azimuth angle, zenith angle, pressure, opaque cloud cover, and total cloud cover. Also, synoptic event detection was applied for learning the underlying influence of the given variables and their features on solar irradiance. The proposed model provided a RMSE of 41.69%, which is equivalent to 149.29 W/m^2.

2) SUPPORT VECTOR MACHINE-BASED MODELS

Belaid and Mellit [88] compared the performance of SVMs and multi-layer perceptron neural networks (MLP-NNs) for the one step ahead daily and monthly predictions of global solar radiation. Several combinations of input variables were examined, including the potential sunshine duration, extraterrestrial global solar radiation (So), and measured ambient temperatures. Table 3 reports the best daily predicted GSR in terms of NRMSE using SVM and MLP-NN which were both trained and tested using the same inputs, namely the minimum, mean and the difference of the ambient temperature, and the daily So. The best performing SVM was set at a regularization parameter of 2172500, and a kernel bandwidth of 8.666. While considering several input combinations, it was concluded that SVMs achieved slightly better results compared to ANN-based approaches. However, for short-term solar power prediction, Zeng and Qiao [87] have shown that the least-square SVM significantly outperformed the AR model and achieved better results compared to radial basis function NN. The inputs of the proposed model included historical two-dimensional atmospheric transmissivity data, and meteorological variables, such as wind speed, relative humidity, in addition to the sky cover which was significant in improving the prediction accuracy. Even though the SVM outperformed the NN in [88] and [87], however, in [86], the SVM achieved higher prediction error compared to the NN. This variation in results is due to the application of different combinations of input parameters, the kernel function, the SVM parameters, the different datasets, along with the different architectures and learning algorithms of the NNs.

3) REGRESSION-BASED MODELS

Martín *et al.* [90] studied the predictability the half daily values of global solar irradiance. Accordingly, two hourly accumulated values over a 3-day time horizon were used, namely solar rise to noon, and noon to solar dawn values of each day (i.e. 6 total values). For overcoming the non-stationary behavior of half daily global solar irradiance, the clearness index (KT) and lost component (LC) stationary variables were derived from the given solar irradiance time series and were used as the inputs of the predictive model. Several orders of autoregressive models (i.e. infinite impulse response filters) were studied along with the NNs trained using Leverage-Marquardt algorithm, and adaptive network based fuzzy inference system (ANFIS). The performance of these models was compared using the relative root mean square deviation (rRMSD), and the improvement factor. Table 3 reports the range of the rRMSDs for the different models at each station over the 6 intervals. It was concluded from [90] the superiority of the nonlinear models compared to the autoregressive models. Correspondingly, the most useful information for prediction lies within the first temporal lag of the time series, and the best results were obtained from the LC time series using NN and ANFIS models, except for one station. However, the KT achieved better results for lower order models. The evaluation process proved the strong dependence of the prediction error on the climatic conditions and the temporal sequence of the training dataset.

Moghaddamnia *et al.* [101] applied the gamma test (GT) for the appropriate selection of input parameters and training data length used for forecasting the daily solar irradiance. Meteorological parameters were applied, such as the daily

average and maximum temperatures, precipitation, wind velocity, and extraterrestrial radiation. Different non-linear modeling approaches were evaluated with the aid of GT, such as local linear regression, Elman NN, MLP trained with Broyden–Fletcher–Goldfarb–Shanno (BFGS), MLP trained with conjugate gradient algorithm, NN autoregressive model with exogenous inputs (NNARX), and ANFIS trained with LM algorithm. The experimental results revealed that local linear regression (LLR) provided the most reliable estimations among the given models. However, the MLP (conjugate gradient) outperformed MLP (BFGS), which both outperformed the Elman and ANFIS models in both the training and the validation periods. From Table 3, the NNARX model presented better prediction accuracy during the training period compared to the MLP models. In conclusion, the ANFIS model was uncompetitive in the solar irradiance forecasting, on the contrast of the LLR and NNARX models, which were more adequate for that purpose.

The performance of several data-driven models for the daily multi-step ahead solar prediction was compared in [103]. These models included the multivariate linear regression (MLR) model, NN, k-nearest neighbor (kNN), and different kernels of SVM. In the first evaluation scenario, meteorological data were considered in addition to the historical data, while in the second scenario, only time-series data was included. The importance of the meteorological parameters was analyzed using linear regression, SVM regression, and pace regression algorithms. The conducted evaluation revealed the superiority of maximum, mean, and minimum temperatures, in addition to the insolation, followed by wind speed and precipitation. The experimental results proved that the time-series models provided better predictions in the multi-steps ahead solar power prediction. Conversely, the meteorological data resulted in more accurate predictions for the current time solar power prediction with MAPE lower than 20% compared to MAPE of more than 30% using time-series models. It was shown that the contribution of meteorological data is of less significance with the increase of the prediction horizon. None of the four data-driven models constantly outperformed the others in all the time-ahead steps.

4) HYBRID MODELS

Other studies have considered applying hybrid ML models. For example, Chen *et al.* [82] proposed a hybrid model for the hourly solar radiation forecasting based on fuzzy logic and NNs, which improved the MAPE by nearly 10% compared to the use of the other techniques individually at the various weather conditions. Parameters including the past and future sky conditions and temperature information were considered in this model. Also, fuzzy logic was applied to optimize the clustering process and reduce the number of classes of these parameters. The MAPE of the proposed model as presented in Table 3 demonstrate its superiority compared to statistical models, and individual fuzzy, and NN approaches.

Voyant *et al.* [89] proposed the integration of AI models and statistical techniques for the hourly global radiation prediction by considering the multi-layer perceptron (MLP), ARMA, and persistence models in that study. The performance of each of these models was evaluated individually in terms of the hourly prediction error and the cumulative prediction error over 24 hours. For the MLP, 6 sub-variables were derived from the given pressure time series, including the minimum, the maximum and the mean pressure of the day, and the daily trend pressure. Using the mutual information method, the daily trend pressure was selected as the variable with the highest dependency on the global radiation and was applied as the input variable of the MLP. Afterward, Bayesian rules were applied to hybridize the evaluated models to improve the performance. The results in Table 3 indicate the equivalence in the hourly prediction NRMSE for both the MLP and ARMA models with nearly 40.5%, which was reduced to 37% using the hybrid model, which considered the previous mean error (PME) rule.

Grigorievskiy *et al.* [104] adopted optimally pruned extreme machine learning (OP-ELM) model for the problem of long-term time series forecasting. Three long-term time series forecasting strategies were considered in integration with the OP-ELM, namely the direct, DirRec, and recursive strategies, which were combined with baseline least square SVM (LS-SVM), and linear least square models for comparison. The results using three datasets have demonstrated that DirRec strategy had the highest computational time, when integrated with LS-SVM, as it requires the adjustment of several hyperparameters. Nevertheless, the same strategy consumed less computational time with the non-linear OP-ELM model, which also outperformed the linear model, and had more stable performance compared to the LS-SVM. It was concluded that adopting an ensemble of OP-ELM would improve the prediction accuracy significantly, as shown in Table 3 in terms of MSE.

Wang *et al.* [86] proposed an adaptive learning hybrid model (ALHM) for both short-term, and long-term forecasting of solar intensity. The ALHM integrated time-varying multiple linear model (TMLM), genetic algorithm back propagation network (GABP), and adaptive learning online hybrid algorithm (ALOHA), as these models capture the linear, dynamic, and nonlinear properties of the collected data, respectively. The input parameters of temperature, dew point, humidity, precipitation, and wind speed were included. The proposed ALHM performance was compared to NN and SVM using a two-year dataset from the UMASS Trace Repository [98] of solar intensity levels (Watts/ m2), and meteorological data, which are recorded for every 5 minutes. The MAPE of the proposed method was compared to the MAPE of NN and SVM in both the long-term (daily) and short-term (5-min), as reported in Table 3. Accordingly, it has established the superiority of the proposed model due to the

deficiency of NN and SVM in analyzing and learning the linear and non-linear relationships of solar power generation and meteorological data in real-life applications.

On the other hand, in unsupervised approaches, unlabeled data are provided to the system model, which analyzes the inherent distribution or structure within the given data samples to distinguish them into different groups. As an example, Feng *et al.* [100] proposed an unsupervised clustering-based (UC-based) global horizontal radiance (GHI) model for the hour-ahead short-term solar prediction. In the proposed model, the daily time series is first clustered using the proposed optimized cross-validated clustering (OCCUR) method, which optimized the number of clusters and the clustering performance. Then, SVM-based pattern recognition was adopted to identify the data category of each day using only the first four hour data. After that, forecasting was performed using M3, a two-layer machine learning-based multi-model, which include NN, SVR, random forests, and gradient boosting machine. The UC-M3 model has proved to achieve better performance than single-algorithm ML (SAML) methods by approximately 20%, as shown in Table 3.

Despite the wide availability of ambient RF signals, the power of the electromagnetic waves rapidly decreases as the signal spreads away from the source. Thus, the RF harvesters should either be placed close to the RF sources, or dedicated RF transmitters can be used merely for the purpose of powering the EH devices. This factor has limited the applicability of RF energy in EH wearables, except for indoor environments, such as harvesting the WiFi signals in office environments [39]. Therefore, few studies have investigated the RF energy prediction, which relies on predicting the quality of the link connectivity, which in turn reflects on the ability of the EH nodes to harvest RF energy. Link quality prediction or RF link duration prediction allows the detection of the remaining node efficient connectivity time for avoiding the unnecessary transmissions of data or control messages. De Araújo *et al.* [63] proposed a genetic machine learning approach for link quality prediction (GMLA) based on a classifier system at which a selected set of classifiers was evolved using the genetic algorithm (GA) after a predetermined set of consults. This approach represented an extension of the oriented birth-death model (OBD) as it relied on Markov Chain model for forecasting the link quality in the future, while also replacing the need of previous history to set the parameters of the Markov model with on-the-fly parameters discovery. The experimental results compared the performance of the GMLA model at 6,8, and 10 states with the BD, Markov transition counting process (MTCP), and GPS in terms of link prediction error at different time-ahead steps. These models were assessed with three mobility models, namely the Manhattan mobility (MM) model, reference point group mobility model, and Gauss-Markov mobility (GMM) model. Table 3 reports the best case using MM model for one step ahead prediction, and the worst case using the GMM mobility model for 30 step ahead prediction. The results depicted that the number of states should be compromised for adequate prediction precision. This proposed approach was an extension of the study in [102] in which the OBD model was proposed for estimating the RF connectivity. The results in Table 3 demonstrate the best and worst prediction cases at one step ahead MM model and 20 steps ahead GMM model, respectively. It is shown that the proposed OBD model achieved better performance using 6 states compared to 8 or 10 states in both cases. Both studies established that the best performance was obtained using the MM model, while representing the link quality by 6 states.

V. DISCUSSION, FUTURE DIRECTIONS & RECOMMENDATIONS

The EH-based medical wearable devices and EH-WSNs exploit mutual energy sources, namely the photovoltaic and RF energy sources, allowing for continuous and sustainable operation. Different energy prediction methods were proposed for estimating the availability of these sources, which include statistical, stochastic and ML-based methods. In statistical methods, historical time-series data is used for energy predictions, however, the selection of slot length presents a tradeoff between the prediction accuracy, which is achieved at shorter slots and the equivalent memory requirement imposed by the large number of slots. Statistical methods have developed throughout different studies in order to adapt to the abrupt weather conditions and fast seasonal changes from EWMA to IPro-Energy. These methods are applicable to short-term, medium-term, and long-term predictions. Since, the variation in the energy harvesting rate throughout the day adversely affect the prediction accuracy, variable length timeslots were proposed to adapt to the dynamics of the energy source. For example, the Pro-Energy-VLT model which outperformed the Pro-Energy and WCMA models in terms of memory requirement, and predictive accuracy for short-term, medium-term, and long-term indoor and outdoor photovoltaic predictions [70].

Stochastic models are based on Markov chain models by defining the states that represent the radiation values. Higher-order Markov chains provide higher prediction accuracy at the expense of the system complexity. Stochastic models propose a less execution time compared to statistical models, however, they achieve less prediction accuracy and more memory requirement, such as the ASIM model compared to the IPro-Energy model [20]. Moreover, stochastic models are not applicable to medium-term predictions, while long-term predictions can be achieved by aggregating the energy values over one day. Physical models such as NWP in addition to satellite-based approaches achieve reasonable prediction results over large temporal and spatial resolutions, however, these methods can hardly achieve precise predictions for intra-hourly and site-specific predictions [91], [92]. Sky imagery-based methods are more adequate for intra-hourly forecasts, however, their performance is limited by the assumptions of cloud shape and linear movement.

On the other hand, machine learning approaches, such as NN are able to automatically adapt to long-term and sudden changes in environmental and climatic conditions. Feed forward and model averaging NN models presented better performance compared to back propagation and deep learning NN models for both hourly and daily solar forecasting. Feedforward NN required less memory compared to model averaged NN and backpropagation NN [83], [84]. However, deep learning models have outperformed NN, Gaussian process regression, and support vector regression for daily average global solar radiation due to the non-linear mapping layer, which exploit the non-linear relationships among the input parameters [85]. Statistical methods, such as ICA can be used to select the most significant meteorological parameters for the ML model [93]. Generally, minimum, maximum, and average daily temperatures in addition to humidity, precipitation, pressure, wind velocity, and cloud cover are considered the most significant for hourly and daily predictions. For SVMs, the selection of the kernel function and regularization parameters is crucial for the optimum performance, while non-linear kernel functions present better performance. The selection of the input parameters for the given dataset and time horizon could lead to different results using the same models, which can be addressed using statistical feature selection methods or regression models [87], [91], [92]. Generally, non-linear models have established higher prediction accuracy compared to regressive models for half daily values of global solar irradiance forecasting [90].

Nevertheless, LLR and NNARX models presented more reliable performance in daily solar irradiance forecasting compared to other non-linear methods [101]. The fuzzy models can improve the performance of the forecasting models by optimizing the data classes clustering process [82]. Hybrid models [82], [87], [88], [98] based on both ML and statistical approaches, and ensembles have shown higher accuracy compared to either approach separately for both short-term and long-term predictions, as these models are able to analyze and learn the linear and non-linear relationships of solar power and meteorological data. Although few studies were proposed for RF forecasting, efficient link quality forecasting was proposed using the GMLA approach, which is based on Markov chain model, as an extension to the OBD model [63]. Table 4 summarizes the main characteristics of the different prediction approaches and compares their accuracy, memory requirement, and execution time.

Several challenging issues still require thorough investigation for fulfilling the wide adoption of EH wearable devices. These issues can be summarized as follows: i) the size and flexibility requirements of EH modules in wearable devices, and the potential advancements in these factors with the nanoscale fabrication technology, while maintaining high output power; ii) the efficient storage of the harvested energy; iii) the tradeoff between the energy prediction accuracy, and the high algorithmic complexity and extensive memory requirement, especially in hybrid prediction methods; and v) the integration of energy prediction models at the different levels of the communication protocol stack to achieve network neutral operation (NNO).

TABLE 4. Summary of the main energy harvesting prediction approaches.

	Statistical	Stochastic	Machine learning				
			NN	SVM	Regression	Ensemble	Hybrid
Prediction accuracy	Average	Below average	Above average	Above average	Average	Highest	Highest
Memory requirements	Low	Low	High	High	High	Highest	Highest
Computational speed	Low	Least	High	High	High	Highest	Highest
Characteristics	Suitable for short-term predictions	Prediction accuracy increase with Markov chains complexity	Suitable for both short-term and long-term predictions at the expense of higher memory and execution time				

From the investigation of the given studies, statistical techniques are recommended for short-term predictions due to their reasonable performance in terms of the tradeoff between the prediction accuracy on one hand, and the memory requirements and execution time on the other hand. However, the hybridization of linear and non-linear ML techniques proposes a better solution for long-term predictions due to its ability to capture both the linear and non-linear patterns of the applied long-term weather parameters.

VI. CONCLUSION

Recent advances in microelectronics, soft computing and AI techniques have fueled the emergence of wearable devices that can be used to monitor vital human signs, detect abnormal behavior or to make the elderly live more independent lives. Together with the introduction of 5G, these intelligent devices are bound to make an enormous impact on the advancement of mobile and personal healthcare. In fact, we have demonstrated that wearable devices resemble EH-WSN nodes in their architectural design and their dependency on conventional or finite energy storage mechanisms, such as batteries and capacitors. We have also indicated that their reliance on such finite storage mechanisms is among the obstacles for a deeper market penetration. Thus, existing wearable technologies cannot be used for continuous and uninterrupted physiological patient monitoring, since batteries need to be replaced or recharged. Consequently, energy harvesting technologies aim to extend or mitigate the limitations of these batteries. However, as we discussed, energy harvesting techniques such as PV, piezoelectric or thermoelectric technologies are either location or time dependent. Moreover, RF energy harvesting technologies yield low power densities. Consequently, the ability for a wearable to forecast or predict the amount of harvestable energy is of paramount importance. In doing so, wearable devices will be able to manage their energy resources more effectively.

Energy prediction techniques have been widely adopted in EH-WSNs for efficient power management and high quality

of service (QoS). However, the application of these methods for wearable devices requires the consideration of several critical parameters that include memory, execution time and prediction accuracy. To maintain maximum comfort for the wearer, these parameters need to be considered to ensure that wearables are small and light weight. Furthermore, wearables need to be low-cost to ensure that they can be adopted by a large tranche of healthcare seekers. In this paper, a comprehensive review of different prediction approaches was provided. The most important evaluation metrics were also discussed. Such metrics aim to provide a baseline or a reference for appropriately selecting the most applicable energy prediction techniques for wearables. These approaches were inspired by EH-WSN prediction techniques, which use the same energy sources as current wearable devices, such as PV and RF sources.

Based on our critical review, we believe that the hybridization of several linear and non-linear ML techniques is a promising domain for long-term predictions in terms of achieving reasonable prediction error. However, the biggest challenge is to optimize the proposed models in terms of required memory and execution time. On the other hand, statistical techniques are the most appropriate method for short-term predictions, since they deliver efficient short-term performance with the least memory and execution time requirements.

ACKNOWLEDGMENT

This work was supported by UK's Engineering and Physical Sciences Research Council (EPSRC) under Grant EP/R511705/1.

REFERENCES

[1] W. H. Organization. (Apr. 19, 2020). *The Global Burden of Chronic*. [Online]. Available: https://www.who.int/nutrition/topics/2_background/en/

[2] M. A. Hanson, H. C. Powell, A. T. Barth, K. Ringgenberg, B. H. Calhoun, J. H. Aylor, and J. Lach, "Body area sensor networks: Challenges and opportunities," *Computer*, vol. 42, no. 1, pp. 58–65, Jan. 2009.

[3] *Wearable Medical Devices Market Worth $139,353.6 Mn by 2026 | Global Market Size, Share, Growth Forecast*, Fortune Business Insights, Pune, India, 2020.

[4] L. J. Hubble and J. Wang, "Sensing at your fingertips: Glove-based wearable chemical sensors," *Electroanalysis*, vol. 31, pp. 428–436, Dec. 2018.

[5] J. Hughes, A. Spielberg, M. Chounlakone, G. Chang, W. Matusik, and D. Rus, "A simple, inexpensive, wearable glove with hybrid resistive-pressure sensors for computational sensing, proprioception, and task identification," *Adv. Intell. Syst.*, vol. 2, no. 6, 2020, Art. no. 2000002.

[6] X. Liang, R. Ghannam, and H. Heidari, "Wrist-worn gesture sensing with wearable intelligence," *IEEE Sensors J.*, vol. 19, no. 3, pp. 1082–1090, Feb. 2019.

[7] X. Liang, H. Li, W. Wang, Y. Liu, R. Ghannam, F. Fioranelli, and H. Heidari, "Fusion of wearable and contactless sensors for intelligent gesture recognition," *Adv. Intell. Syst.*, vol. 1, no. 7, Nov. 2019, Art. no. 1900088.

[8] T. Takamatsu, Y. Chen, T. Yoshimasu, M. Nishizawa, and T. Miyake, "Highly efficient, flexible wireless-powered circuit printed on a moist, soft contact lens," *Adv. Mater. Technol.*, vol. 4, no. 5, May 2019, Art. no. 1800671.

[9] M. Yuan, R. Das, R. Ghannam, Y. Wang, J. Reboud, R. Fromme, F. Moradi, and H. Heidari, "Electronic contact lens: A platform for wireless health monitoring applications," *Adv. Intell. Syst.*, vol. 2, no. 4, Apr. 2020, Art. no. 1900190.

[10] M. Magno, G. A. Salvatore, P. Jokic, and L. Benini, "Self-sustainable smart ring for long-term monitoring of blood oxygenation," *IEEE Access*, vol. 7, pp. 115400–115408, 2019.

[11] X. Zhang, K. Kadimisetty, K. Yin, C. Ruiz, M. G. Mauk, and C. Liu, "Smart ring: A wearable device for hand hygiene compliance monitoring at the point-of-need," *Microsyst. Technol.*, vol. 25, no. 8, pp. 3105–3110, Aug. 2019.

[12] B. Gyselinckx, C. Van Hoof, J. Ryckaert, R. F. Yazicioglu, P. Fiorini, and V. Leonov, "Human++: Autonomous wireless sensors for body area networks," in *Proc. IEEE Custom Integr. Circuits Conf.*, Sep. 2005, pp. 13–19.

[13] T. B. Reddy, *Linden's Handbook of Batteries*, vol. 4. New York, NY, USA: McGraw-Hill, 2011.

[14] T. Ghomian and S. Mehraeen, "Survey of energy scavenging for wearable and implantable devices," *Energy*, vol. 178, pp. 33–49, Jul. 2019.

[15] S. Basagni, M. Y. Naderi, C. Petrioli, D. Spenza, M. Conti, S. Giordano, and I. Stojmenovic, "Wireless sensor networks with energy harvesting," in *Mobile Ad Hoc Networking: Cutting Edge Directions*, S. Basagni, M. Conti, S. Giordano, and I. Stojmenovic, Eds. Hoboken, NJ, USA: Wiley, 2013, pp. 703–736.

[16] D. Lau, N. Song, C. Hall, Y. Jiang, S. Lim, I. Perez-Wurfl, Z. Ouyang, and A. Lennon, "Hybrid solar energy harvesting and storage devices: The promises and challenges," *Mater. Today Energy*, vol. 13, pp. 22–44, Sep. 2019.

[17] L. M. Borges, F. J. Velez, N. Barroca, R. Chávez-Santiago, and I. Balasingham, "Radio-frequency energy harvesting for wearable sensors," *Healthcare Technol. Lett.*, vol. 2, no. 1, pp. 22–27, Feb. 2015.

[18] A. Nozariasbmarz, H. Collins, K. Dsouza, M. H. Polash, M. Hosseini, M. Hyland, J. Liu, A. Malhotra, F. M. Ortiz, F. Mohaddes, V. P. Ramesh, Y. Sargolzaeiaval, N. Snouwaert, M. C. Özturk, and D. Vashaee, "Review of wearable thermoelectric energy harvesting: From body temperature to electronic systems," *Appl. Energy*, vol. 258, Jan. 2020, Art. no. 114069.

[19] S. Chandrasekaran, C. Bowen, J. Roscow, Y. Zhang, D. K. Dang, E. J. Kim, R. D. K. Misra, L. Deng, J. S. Chung, and S. H. Hur, "Micro-scale to nano-scale generators for energy harvesting: Self powered piezoelectric, triboelectric and hybrid devices," *Phys. Rep.*, vol. 792, pp. 1–33, Feb. 2019.

[20] H. K. Qureshi, U. Saleem, M. Saleem, A. Pitsillides, and M. Lestas, "Harvested energy prediction schemes for wireless sensor networks: Performance evaluation and enhancements," *Wireless Commun. Mobile Comput.*, vol. 2017, pp. 1–14, Oct. 2017.

[21] F. K. Shaikh and S. Zeadally, "Energy harvesting in wireless sensor networks: A comprehensive review," *Renew. Sustain. Energy Rev.*, vol. 55, pp. 1041–1054, Mar. 2016.

[22] N. B. Bharatula, P. Lukowicz, and G. Tröster, "Functionality-power-packaging considerations in context aware wearable systems," *Pers. Ubiquitous Comput.*, vol. 12, no. 2, pp. 123–141, Feb. 2008.

[23] T. N. Le, A. Pegatoquet, O. Berder, and O. Sentieys, "Multi-source power manager for super-capacitor based energy harvesting WSN," in *Proc. 1st Int. Workshop Energy Neutral Sens. Syst. (ENSSys)*, 2013, pp. 1–2.

[24] D. Brunelli, "Miniaturized solar scavengers for ultra-low power wireless sensor nodes," in *Proc. WEWSN*, 2008.

[25] F. Simjee, D. Sharma, and P. H. Chou, "Everlast: Long-life, supercapacitor-operated wireless sensor node," in *Proc. 3rd Int. Conf. Embedded Networked sensor Syst. (SenSys)*, 2005, pp. 197–202.

[26] T. N. Le, A. Pegatoquet, O. Berder, and O. Sentieys, "Energy-efficient power manager and MAC protocol for multi-hop wireless sensor networks powered by periodic energy harvesting sources," *IEEE Sensors J.*, vol. 15, no. 12, pp. 7208–7220, Dec. 2015.

[27] T. Zhu, Z. Zhong, Y. Gu, T. He, and Z.-L. Zhang, "Leakage-aware energy synchronization for wireless sensor networks," in *Proc. 7th Int. Conf. Mobile Syst., Appl., Services (Mobisys)*, 2009, pp. 319–332.

[28] M. Thielen, L. Sigrist, M. Magno, C. Hierold, and L. Benini, "Human body heat for powering wearable devices: From thermal energy to application," *Energy Convers. Manage.*, vol. 131, pp. 44–54, Jan. 2017.

[29] R. Arai, S. Furukawa, N. Sato, and T. Yasuda, "Organic energy-harvesting devices achieving power conversion efficiencies over 20% under ambient indoor lighting," *J. Mater. Chem. A*, vol. 7, no. 35, pp. 20187–20192, 2019.

[30] X. Ma, S. Bader, and B. Oelmann, "Power estimation for indoor light energy harvesting systems," *IEEE Trans. Instrum. Meas.*, early access, Mar. 30, 2020, doi: 10.1109/TIM.2020.2984145.

[31] C. Li, S. Cong, Z. Tian, Y. Song, L. Yu, C. Lu, Y. Shao, J. Li, G. Zou, M. H. Rümmeli, S. Dou, J. Sun, and Z. Liu, "Flexible perovskite solar cell-driven photo-rechargeable lithium-ion capacitor for self-powered wearable strain sensors," *Nano Energy*, vol. 60, pp. 247–256, Jun. 2019.

[32] S. A. Hashemi, S. Ramakrishna, and A. G. Aberle, "Recent progress in flexible–wearable solar cells for self-powered electronic devices," *Energy Environ. Sci.*, vol. 13, no. 3, pp. 685–743, 2020.

[33] H. Mamur, M. R. A. Bhuiyan, F. Korkmaz, and M. Nil, "A review on bismuth telluride (Bi_2Te_3) nanostructure for thermoelectric applications," *Renew. Sustain. Energy Rev.*, vol. 82, pp. 4159–4169, Feb. 2018.

[34] P. D. Mitcheson, "Energy harvesting for human wearable and implantable bio-sensors," in *Proc. Annu. Int. Conf. IEEE Eng. Med. Biol.*, Aug. 2010, pp. 3432–3436.

[35] K. Tao, H. Yi, L. Tang, J. Wu, P. Wang, N. Wang, L. Hu, Y. Fu, J. Miao, and H. Chang, "Piezoelectric ZnO thin films for 2DOF MEMS vibrational energy harvesting," *Surf. Coatings Technol.*, vol. 359, pp. 289–295, Feb. 2019.

[36] H. Shi, Z. Liu, and X. Mei, "Overview of human walking induced energy harvesting technologies and its possibility for walking robotics," *Energies*, vol. 13, no. 1, p. 86, Dec. 2019.

[37] T. Starner, "Human-powered wearable computing," *IBM Syst. J.*, vol. 35, nos. 3–4, pp. 618–629, 1996.

[38] N. S. Shenck and J. A. Paradiso, "Energy scavenging with shoe-mounted piezoelectrics," *IEEE Micro*, vol. 21, no. 3, pp. 30–42, May/Jun. 2001.

[39] V. H. Tran, A. Misra, J. Xiong, and R. K. Balan, "WiWear: Wearable sensing via directional WiFi energy harvesting," in *Proc. IEEE Int. Conf. Pervas. Comput. Commun. (PerCom)*, Mar. 2019, pp. 1–10.

[40] X. Zhang, J. Grajal, J. L. Vazquez-Roy, U. Radhakrishna, X. Wang, W. Chern, L. Zhou, Y. Lin, P.-C. Shen, X. Ji, X. Ling, A. Zubair, Y. Zhang, H. Wang, M. Dubey, J. Kong, M. Dresselhaus, and T. Palacios, "Two-dimensional MoS2-enabled flexible rectenna for Wi-Fi-band wireless energy harvesting," *Nature*, vol. 566, no. 7744, pp. 368–372, Feb. 2019.

[41] M. A. Halim, R. Rantz, Q. Zhang, L. Gu, K. Yang, and S. Roundy, "Electromagnetic energy harvesting from swing-arm motion using rotational eccentric mass structure," in *Proc. 19th Int. Conf. Solid-State Sensors, Actuat. Microsys. (TRANSDUCERS)*, Jun. 2017, pp. 1863–1866.

[42] M. A. Halim, R. Rantz, Q. Zhang, L. Gu, K. Yang, and S. Roundy, "An electromagnetic rotational energy harvester using sprung eccentric rotor, driven by pseudo-walking motion," *Appl. Energy*, vol. 217, pp. 66–74, May 2018.

[43] M. Magno, X. Wang, M. Eggimann, L. Cavigelli, and L. Benini, "Infini-Wolf: Energy efficient smart bracelet for edge computing with dual source energy harvesting," in *Proc. Design, Autom. Test Eur. Conf. Exhib. (DATE)*, Grenoble, France, Mar. 2020, pp. 1–4.

[44] M. S. Costa, L. T. Manera, and H. S. Moreira, "Study of the light energy harvesting capacity in indoor environments," in *Proc. 4th Int. Symp. Instrum. Syst., Circuits Transducers (INSCIT)*, Aug. 2019, pp. 1–4.

[45] T. Tomono, "A new approach for body heat energy harvesting," *Int. J. Energy Res.*, vol. 43, no. 9, pp. 4967–4975, Jul. 2019.

[46] S. Tiwari, A. Gaur, C. Kumar, and P. Maiti, "Enhanced piezoelectric response in nanoclay induced electrospun PVDF nanofibers for energy harvesting," *Energy*, vol. 171, pp. 485–492, Mar. 2019.

[47] F. Wu, C. Li, Y. Yin, R. Cao, H. Li, X. Zhang, S. Zhao, J. Wang, B. Wang, Y. Xing, and X. Du, "A flexible, lightweight, and wearable triboelectric nanogenerator for energy harvesting and self-powered sensing," *Adv. Mater. Technol.*, vol. 4, Jan. 2019, Art. no. 1800216.

[48] M. A. Green, E. D. Dunlop, D. H. Levi, J. Hohl-Ebinger, M. Yoshita, and A. W. Ho-Baillie, "Solar cell efficiency tables (version 54)," *Prog. Photovoltaics, Res. Appl.*, vol. 27, pp. 565–575, Jul. 2019.

[49] M. Magno, X. Wang, M. Eggimann, L. Cavigelli, and L. Benini, "Infini-Wolf: Energy efficient smart bracelet for edge computing with dual source energy harvesting," 2020, *arXiv:2003.00041*. [Online]. Available: http://arxiv.org/abs/2003.00041

[50] P. Jokic and M. Magno, "Powering smart wearable systems with flexible solar energy harvesting," in *Proc. IEEE Int. Symp. Circuits Syst. (ISCAS)*, May 2017, pp. 1–4.

[51] B. Balachander, S. Sinthamani, and S. Sudharsanam, "Solar powered DC–DC converter for wearable devices," in *Proc. 4th Int. Conf. Electr. Energy Syst. (ICEES)*, Feb. 2018, pp. 425–432.

[52] V. Kartsch, S. Benatti, M. Mancini, M. Magno, and L. Benini, "Smart wearable wristband for EMG based gesture recognition powered by solar energy harvester," in *Proc. IEEE Int. Symp. Circuits Syst. (ISCAS)*, May 2018, pp. 1–5.

[53] B. Naresh, V. K. Singh, V. Bhargavi, A. Garg, and A. K. Bhoi, "Dual-band wearable rectenna for low-power RF energy harvesting," in *Proc. Adv. Power Syst. Energy Manage.* Singapore: Springer, 2018, pp. 13–21.

[54] M. M. Mansour and H. Kanaya, "Development of compact and high-efficient simple CPW rectenna for RF energy harvesting," in *Proc. Int. Conf. Electron. Packag. (ICEP)*, Apr. 2019, pp. 130–133.

[55] A. Sharma and A. Kakkar, "Forecasting daily global solar irradiance generation using machine learning," *Renew. Sustain. Energy Rev.*, vol. 82, pp. 2254–2269, Feb. 2018.

[56] H. Chu, H. Jang, Y. Lee, Y. Chae, and J.-H. Ahn, "Conformal, graphene-based triboelectric nanogenerator for self-powered wearable electronics," *Nano Energy*, vol. 27, pp. 298–305, Sep. 2016.

[57] C. S. Kim, H. M. Yang, J. Lee, G. S. Lee, H. Choi, Y. J. Kim, S. H. Lim, S. H. Cho, and B. J. Cho, "Self-powered wearable electrocardiography using a wearable thermoelectric power generator," *ACS Energy Lett.*, vol. 3, no. 3, pp. 501–507, Mar. 2018.

[58] N. H. H. Mohamad Hanif, A. Jazlan Mohaideen, H. Azam, and M. E. Rohaimi, "Rotational piezoelectric energy harvester for wearable devices," *Cogent Eng.*, vol. 5, no. 1, Jan. 2018, Art. no. 1430497.

[59] D. Sengupta and A. G. P. Kottapalli, "Flexible and wearable piezoelectric nanogenerators," in *Self-Powered and Soft Polymer MEMS/NEMS Devices*. Cham, Switzerland: Springer, 2019, pp. 31–60.

[60] K. A. Sunitha, S. Dixit, and P. Singh, "Design and development of a self-powered wearable device for a tele-medicine application," *Wireless Pers. Commun.*, vol. 108, no. 1, pp. 175–186, Sep. 2019.

[61] M. F. Mahmood, S. L. Mohammed, and S. K. Gharghan, "Energy harvesting-based vibration sensor for medical electromyography device," *Int. J. Electr. Electron. Eng. Telecommun*, vol. 9, Jan. 2020.

[62] H. H. R. Sherazi, L. A. Grieco, and G. Boggia, "A comprehensive review on energy harvesting MAC protocols in WSNs: Challenges and tradeoffs," *Ad Hoc Netw.*, vol. 71, pp. 117–134, Mar. 2018.

[63] G. M. de Araújo, A. R. Pinto, J. Kaiser, and L. B. Becker, "Genetic machine learning approach for link quality prediction in mobile wireless sensor networks," in *Cooperative Robots and Sensor Networks*. Berlin, Germany: Springer, 2014, pp. 1–18.

[64] A. Kansal, J. Hsu, S. Zahedi, and M. B. Srivastava, "Power management in energy harvesting sensor networks," *ACM Trans. Embedded Comput. Syst.*, vol. 6, no. 4, p. 32, Sep. 2007.

[65] D. R. Cox, "Prediction by exponentially weighted moving averages and related methods," *J. Roy. Stat. Soc. B, Methodol.*, vol. 23, no. 2, pp. 414–422, Jul. 1961.

[66] S. Kosunalp, "An energy prediction algorithm for wind-powered wireless sensor networks with energy harvesting," *Energy*, vol. 139, pp. 1275–1280, Nov. 2017.

[67] C. Bergonzini, D. Brunelli, and L. Benini, "Comparison of energy intake prediction algorithms for systems powered by photovoltaic harvesters," *Microelectron. J.*, vol. 41, no. 11, pp. 766–777, Nov. 2010.

[68] J. R. Piorno, C. Bergonzini, D. Atienza, and T. S. Rosing, "Prediction and management in energy harvested wireless sensor nodes," in *Proc. 1st Int. Conf. Wireless Commun., Veh. Technol., Inf. Theory Aerosp. Electron. Syst. Technol.*, 2009, pp. 6–10.

[69] A. H. Dehwah, S. Elmetennani, and C. Claudel, "UD-WCMA: An energy estimation and forecast scheme for solar powered wireless sensor networks," *J. Netw. Comput. Appl.*, vol. 90, pp. 17–25, Jul. 2017.

[70] A. Cammarano, C. Petrioli, and D. Spenza, "Online energy harvesting prediction in environmentally powered wireless sensor networks," *IEEE Sensors J.*, vol. 16, no. 17, pp. 6793–6804, Sep. 2016.

[71] M. Muselli, P. Poggi, G. Notton, and A. Louche, "First order Markov chain model for generating synthetic 'typical days' series of global irradiation in order to design photovoltaic stand alone systems," *Energy Convers. Manage.*, vol. 42, no. 6, pp. 675–687, 2001.

[72] A. Seyedi and B. Sikdar, "Modeling and analysis of energy harvesting nodes in wireless sensor networks," in *Proc. 46th Annu. Allerton Conf. Commun., Control, Comput.*, Sep. 2008, pp. 67–71.

[73] J. Ventura and K. Chowdhury, "Markov modeling of energy harvesting body sensor networks," in *Proc. IEEE 22nd Int. Symp. Pers., Indoor Mobile Radio Commun.*, Sep. 2011, pp. 2168–2172.

[74] S. Zhang and A. Seyedi, "Analysis and design of energy harvesting wireless sensor networks with linear topology," in *Proc. IEEE Int. Conf. Commun. (ICC)*, Jun. 2011, pp. 1–5.

[75] M.-L. Ku, Y. Chen, and K. J. Ray Liu, "Data-driven stochastic models and policies for energy harvesting sensor communications," *IEEE J. Sel. Areas Commun.*, vol. 33, no. 8, pp. 1505–1520, Aug. 2015.

[76] M. F. Ghuman, A. Iqbal, H. K. Qureshi, and M. Lestas, "ASIM: Solar energy availability model for wireless sensor networks," in *Proc. 3rd Int. Workshop Energy Harvesting Energy Neutral Sens. Syst. (ENSsys)*, 2015, pp. 21–26.
[77] P. Lee, Z. A. Eu, M. Han, and H.-P. Tan, "Empirical modeling of a solar-powered energy harvesting wireless sensor node for time-slotted operation," in *Proc. IEEE Wireless Commun. Netw. Conf.*, Mar. 2011, pp. 179–184.
[78] L. Tan and S. Tang, "Energy harvesting wireless sensor node with temporal death: Novel models and analyses," *IEEE/ACM Trans. Netw.*, vol. 25, no. 2, pp. 896–909, Apr. 2017.
[79] A. Sharma and A. Kakkar, "A review on solar forecasting and power management approaches for energy-harvesting wireless sensor networks," *Int. J. Commun. Syst.*, vol. 33, no. 8, p. e4366, May 2020.
[80] F. Ait Aoudia, M. Gautier, and O. Berder, "RLMan: An energy manager based on reinforcement learning for energy harvesting wireless sensor networks," *IEEE Trans. Green Commun. Netw.*, vol. 2, no. 2, pp. 408–417, Jun. 2018.
[81] R. C. Hsu, C.-T. Liu, and H.-L. Wang, "A reinforcement learning-based ToD provisioning dynamic power management for sustainable operation of energy harvesting wireless sensor node," *IEEE Trans. Emerg. Topics Comput.*, vol. 2, no. 2, pp. 181–191, Jun. 2014.
[82] S. X. Chen, H. B. Gooi, and M. Q. Wang, "Solar radiation forecast based on fuzzy logic and neural networks," *Renew. Energy*, vol. 60, pp. 195–201, Dec. 2013.
[83] R. Srivastava, A. N. Tiwari, and V. K. Giri, "Forecasting of solar radiation in india using various ANN models," in *Proc. 5th IEEE Uttar Pradesh Sect. Int. Conf. Electr., Electron. Comput. Eng. (UPCON)*, Nov. 2018, pp. 1–6.
[84] S. Dhillon, C. Madhu, D. Kaur, and S. Singh, "A solar energy forecast model using neural networks: Application for prediction of power for wireless sensor networks in precision agriculture," *Wireless Pers. Commun.*, vol. 11, pp. 1–20, Mar. 2020.
[85] S. Dey, S. Pratiher, S. Banerjee, and C. K. Mukherjee, "SolarisNet: A deep regression network for solar radiation prediction," 2017, *arXiv:1711.08413*. [Online]. Available: http://arxiv.org/abs/1711.08413
[86] Y. Wang, Y. Shen, S. Mao, G. Cao, and R. M. Nelms, "Adaptive learning hybrid model for solar intensity forecasting," *IEEE Trans. Ind. Informat.*, vol. 14, no. 4, pp. 1635–1645, Apr. 2018.
[87] J. Zeng and W. Qiao, "Short-term solar power prediction using a support vector machine," *Renew. Energy*, vol. 52, pp. 118–127, Apr. 2013.
[88] S. Belaid and A. Mellit, "Prediction of daily and mean monthly global solar radiation using support vector machine in an arid climate," *Energy Convers. Manage.*, vol. 118, pp. 105–118, Jun. 2016.
[89] C. Voyant, C. Darras, M. Muselli, C. Paoli, M.-L. Nivet, and P. Poggi, "Bayesian rules and stochastic models for high accuracy prediction of solar radiation," *Appl. Energy*, vol. 114, pp. 218–226, Feb. 2014.
[90] L. Martín, L. F. Zarzalejo, J. Polo, A. Navarro, R. Marchante, and M. Cony, "Prediction of global solar irradiance based on time series analysis: Application to solar thermal power plants energy production planning," *Sol. Energy*, vol. 84, no. 10, pp. 1772–1781, Oct. 2010.
[91] W. Glassley, J. Kleissl, C. P. van Dam, H. Shiu, J. Huang, G. Braun, and R. Holland, "Current state of the art in solar forecasting," Final Rep., Appendix A, California Renew, 2012.
[92] P. Mathiesen and J. Kleissl, "Evaluation of numerical weather prediction for intra-day solar forecasting in the continental united states," *Sol. Energy*, vol. 85, no. 5, pp. 967–977, May 2011.
[93] Y. S. Manjili, R. Vega, and M. M. Jamshidi, "Data-Analytic-Based adaptive solar energy forecasting framework," *IEEE Syst. J.*, vol. 12, no. 1, pp. 285–296, Mar. 2018.
[94] B. M. Alluhaidah, S. H. Shehadeh, and M. E. El-Hawary, "Most influential variables for solar radiation forecasting using artificial neural networks," in *Proc. IEEE Electr. Power Energy Conf.*, Nov. 2014, pp. 71–75.
[95] (2011). *Measurement and Instrumentation Data Center (MIDC)*. [Online]. Available: https://midcdmz.nrel.gov/
[96] M. Gorlatova, A. Wallwater, and G. Zussman, "Networking low-power energy harvesting devices: Measurements and algorithms," *IEEE Trans. Mobile Comput.*, vol. 12, no. 9, pp. 1853–1865, Sep. 2013.
[97] (2011). *National Renewable Energy Laboratory*. [Online]. Available: https://www.nrel.gov/gis/data-tools.html
[98] P. S. M. Liberatore. *The UMass Trace Repository*. Accessed: Jul. 15, 2020. [Online]. Available: http://traces.cs.umass.edu/
[99] A. Hasni, A. Sehli, B. Draoui, A. Bassou, and B. Amieur, "Estimating global solar radiation using artificial neural network and climate data in the south-western region of Algeria," *Energy Procedia*, vol. 18, pp. 531–537, Jan. 2012.
[100] C. Feng, M. Cui, B.-M. Hodge, S. Lu, H. F. Hamann, and J. Zhang, "Unsupervised clustering-based short-term solar forecasting," *IEEE Trans. Sustain. Energy*, vol. 10, no. 4, pp. 2174–2185, Oct. 2019.
[101] A. Moghaddamnia, R. Remesan, M. H. Kashani, M. Mohammadi, D. Han, and J. Piri, "Comparison of LLR, MLP, elman, NNARX and ANFIS models—With a case study in solar radiation estimation," *J. Atmos. Solar-Terr. Phys.*, vol. 71, nos. 8–9, pp. 975–982, Jun. 2009.
[102] G. M. de Araujo, J. Kaiser, and L. B. Becker, "An optimized Markov model to predict link quality in mobile wireless sensor networks," in *Proc. IEEE Symp. Comput. Commun. (ISCC)*, Jul. 2012, pp. 000307–000312.
[103] H. Long, Z. Zhang, and Y. Su, "Analysis of daily solar power prediction with data-driven approaches," *Appl. Energy*, vol. 126, pp. 29–37, Aug. 2014.
[104] A. Grigorievskiy, Y. Miche, A.-M. Ventelä, E. Séverin, and A. Lendasse, "Long-term time series prediction using OP-ELM," *Neural Netw.*, vol. 51, pp. 50–56, Mar. 2014.

MARAM A. WAHBA received the B.Sc. and M.Sc. degrees in electrical engineering from the Faculty of Engineering, Tanta University, Egypt, in 2013. She is currently an Assistant Lecturer with the Department of Electronics and Electrical Communications, Faculty of Engineering, Tanta University. Her research areas include machine learning, pattern recognition, image processing, and medical imaging.

AMIRA S. ASHOUR received the M.Sc. degree in electrical engineering (image processing based nondestructive evaluation performance) and the Ph.D. degree in smart antenna from the Department of Electronics and Electrical Communications Engineering, Faculty of Engineering, Tanta University, Egypt. She is currently an Assistant Professor and has been the Head of the Department of Electronics and Electrical Communications Engineering, Faculty of Engineering, Tanta University, since 2016. She is the ICT Manager of the Huawei Academy, Tanta University. She is an Research and Development member of the Faculty of Engineering, Tanta University. She was the Vice Chair of the Computer Science Department, CIT College, Taif University, Saudi Arabia, from 2009 to 2015. Her research topics are medical devices, image and signal processing, medical imaging, ablation therapy, machine learning, optimization, smart antenna, target tracking, and direction of arrival estimation. She is an Associate Editor of *International Journal of Rough Sets and Data Analysis*, as well as *International Journal of Ambient Computing and Intelligence*. She is an Editorial Board Member of several reputable journals. She published 91 journal articles and conference proceedings and edited/ authored about 20 books (Elsevier/ Springer).

RAMI GHANNAM (Senior Member, IEEE) received the B.Eng. degree in electronic engineering from the King's College and was awarded the Siemens Prize, the D.I.C. and M.Sc. degrees from Imperial College London, and the Ph.D. degree from the University of Cambridge, in 2007. He is currently a Lecturer (Assistant Professor) in electronic and nanoscale engineering with the University of Glasgow. He held previous industrial positions at Nortel Networks and IBM Research GmbH. His research interests are in energy harvesters and engineering education. He is a Senior Fellow of Glasgow's RET scheme and serves as a Scotland's Regional Chair of the IEEE Education Society.